

Dynamics of Water–Ice Grains Formed in a Plasma Where Gravitational Force is Compensated by Thermophoretic Force

Kil-Byoung Chai 

Abstract—A capacitively coupled discharge source equipped with liquid nitrogen cooling system has been developed to create water–ice grains in a plasma environment at the Korea Atomic Energy Research Institute. We found that the gravitational force exerted on 5- μm water–ice grains is nearly compensated by the thermophoretic force when the upper electrode is cooler than that of the bottom electrode by 10–15 K and we observed two distinct, axisymmetric vortex flows are formed in the upper and lower parts of the plasma. The numerical calculation solving a set of equations including the vorticity equation confirms that the observed axisymmetric vortices result from the nonconservative ion drag force.

Index Terms—Plasma applications, plasma devices, plasma measurement, plasmas.

I. INTRODUCTION

PLASMAS containing water–ice grains are ubiquitous; Earth polar mesospheric clouds [1], Saturn’s diffusive rings [2], and comet tails [3] are notable examples. These plasmas have several common features that water–ice grains coexist with electrons, ions, and neutral particles, and water vapor is continuously supplied into the system.

Polar mesospheric clouds form during the summer in the polar region at an altitude of 80–90 km. These clouds consist of electrons, ions, air, and water–ice particles. It is generally accepted that water–ice heterogeneously nucleates on meteoric smoke particles [4] and water–ice particles grow by accreting water molecules around them up to 100 nm [5]. Since the number densities of water–ice particles and ions have a similar order of magnitude, ice particles are not highly charged; most of them are charged with few electrons while some of them (small particles in particular) are charged positively due to the photoemission by solar UV photons [6].

Saturn’s E-, F-, and G-rings are considered as dusty plasmas and are composed of plasma particles and dust particles ranging from few nanometers to few hundreds of μm [2]. (A- and B-rings are not considered as dusty plasmas because

dusts there are too large.) Ions and neutral particles consist of oxygen, hydrogen, water, and helium [7], [8] and most of the dust particles in the Saturn’ rings are made of water–ice. Saturn’s E-ring has gained recent attention owing to its icy moon, Enceladus. Enceladus continuously emits water vapor and water–ice grains to the E-ring via cryovolcanic activities from the tiger stripes in the south pole region [9].

Comet tails are also a good example of dusty plasmas. Solar winds continuously provide electrons and ions to the comet and cause photoionization of cometary neutral species. Volatile materials including water vapor are sublimated from the surface of the nucleus when the nucleus is heated up by solar radiation as it approaches the Sun [10]. Small dust grains, mainly made of water–ice, are lifted off from the nucleus surface by the electrostatic force exerted on the charged grain or by outflowing cometary gas [3]. Water–ice grains in the comet tail are negatively charged if the comet is far from the Sun [11] while they are positively charged due to the photoemission by solar UV photons if the comet is close to the Sun [12].

However, since these plasmas are far from us it is difficult to directly observe the growth and dynamics of water–ice grains. One way to study the growth and dynamics of water–ice grains would be to use a laboratory experiment; a laboratory experiment is beneficial because systemic studies can be carried out with state-of-the-art diagnostics. For this purpose, the Caltech ice dusty plasma experiment was built in 2013 [13]. Since then, several interesting findings have been reported including: 1) spontaneous nucleation takes place without nucleating agents [13]; 2) nonspherical growth occurs when the mean free path of water molecules exceeds the electron Debye length [14]; 3) ice grains formed in a plasma environment have a fractal nature and line up along the electric field [15]; and 4) accretion growth is likely dominant over agglomeration growth [16].

There are several open questions in these communities, namely, how water–ice grains form and grow, how the shape of the water–ice grains affects the charging and dynamics [17], and how they interact with solar winds and surrounding electromagnetic fields [3]. In order to address these issues, a lab experiment similar to the Caltech experiment has been developed at the Korea Atomic Energy Research Institute (KAERI). Besides the dusty plasma issues, the KAERI experiment has been used to study plasma spectroscopy and atomic data and so several plasma diagnostics including an RF compensated Langmuir probe and an absolutely calibrated spectrometer are

Manuscript received June 28, 2017; revised September 29, 2017; accepted October 10, 2017. Date of publication October 24, 2017; date of current version April 10, 2018. This work was supported by the National Research and Development Program through the Korean Ministry of Science, ICT & Future Planning. The review of this paper was arranged by Senior Editor T. Hyde.

The author is with the Nuclear Data Center, Korea Atomic Energy Research Institute, Daejeon 34057, South Korea (e-mail: kbchai@kaeri.re.kr).

This paper has supplementary downloadable material available at <http://ieeexplore.ieee.org>, provided by the author.

Color versions of one or more of the figures in this paper are available online at <http://ieeexplore.ieee.org>.

Digital Object Identifier 10.1109/TPS.2017.2762629

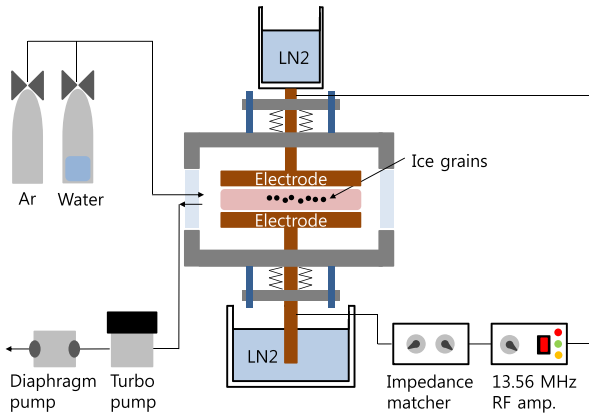


Fig. 1. Sketch of KAERI experiment.

equipped. The initial operation was successfully carried out in 2016 and now water-ice grains are routinely produced in a plasma environment. An interesting feature of the KAERI experiment is that the upper electrode is typically cooler than that of the bottom electrode and these results in the upward thermophoretic force which can be used to compensate the downward gravitational force. The details of the KAERI experiment and the dynamics of water-ice grains are discussed in this paper.

II. EXPERIMENTAL SETUP

A sketch of the KAERI water-ice dusty plasma experiment is shown in Fig. 1 which illustrates a conventional capacitively coupled discharge source with a liquid nitrogen cooling system, similar to the Caltech experiment [13]. The diameter of the copper electrodes is 6 cm and the distance between the electrodes can be adjustable to between 0–4 cm. Guard rings made of aluminum are placed around the electrodes to trap ice (dust) particles. A 13.56-MHz RF generator (YSR-06AF, Youngsin RF) and an automatic matching network (AMN-100A, Youngsin RF) are connected to the electrodes in the push-pull configuration; the bottom electrode is connected to the shielding part of the RF cable and the top electrode is connected to the core of the RF cable while the chamber is grounded. The push-pull configuration is beneficial to achieve vertically symmetric plasmas in which the top and bottom sheaths have the same thickness. The self-bias configuration, on the other hand, can be achieved by connecting the bottom electrode to the vacuum chamber, which leads to a large negative self-bias voltage at the powered electrode; asymmetric sheaths and dust clouds are formed.

In the operation, the bottom electrode is dipped into a liquid nitrogen-filled dewar and the top electrode is directly attached to a copper container holding liquid nitrogen so that it can be cooled down to below 150 K. The temporal behavior of the surface temperature of the top and bottom electrodes after the liquid nitrogen is poured into the bottom dewar and top container is depicted in Fig. 2; the measurements were made using Resistance Temperature Detectors (RTDs) at atmospheric pressure and therefore the electrode surface temperatures might be lower than the values shown in Fig. 2 when

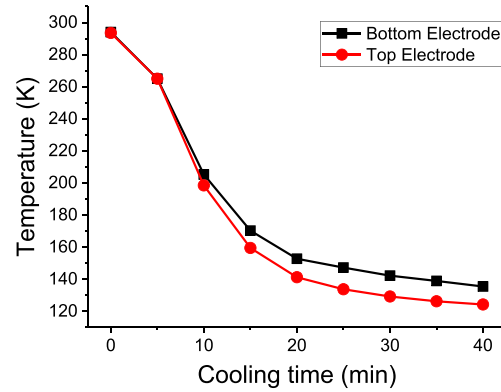


Fig. 2. Temporal behavior of the electrode temperatures after liquid nitrogen is poured into the bottom dewar and the top container.

the chamber is under vacuum. Fig. 2 also reveals that it takes about 30 min. to achieve 150 K for the both electrodes.

After the electrodes are cooled down below 150 K, Ar gas is filled the chamber at 100–600 mTorr and 1–3 W of RF power is applied to ignite a plasma. Then, water vapor is directly injected into the plasma. When the amount of injected water vapor is larger than a certain value, the nucleation of water-ice grains spontaneously takes place. After the nucleation, water-ice grains grow with time and the growth process then stops for an unknown reason within a few minutes.

In order to measure the size and density of water-ice grains, a green diode laser centered at 532 nm is used to illuminate the water-ice grains and the scattered light from the ice grains is measured using a digital single-lens reflex (SLR) camera (EOS 600D, Canon) and a telephoto lens (EF-S 55-250 mm, Canon). The optical resolution of our diagnostic system is 8 μm which was obtained by taking a picture of a microscope target, and thus we are not able to determine the size of particles smaller than 8 μm . The temporal behaviors of water-ice grains are recorded by a digital SLR camera as a movie at a rate of 50 frames per second and sequential images of the movies were used to study the dynamics of the ice grains.

III. RESULTS AND DISCUSSION

A. Nucleation and Growth of Water-Ice Grains

Chai and Bellan reported water-ice grains spontaneously nucleate in a plasma if the water vapor partial pressure is higher than a certain value which is proportional to the input RF power and is inversely proportional to the ambient gas pressure [13], [14]. In the KAERI experiment, the same phenomena are observed. The homogeneous nucleation takes place without nucleating agents and the nucleation only occurs when the water vapor partial pressure is higher than a certain value.

After the nucleation, water-ice grains grow with time. It is observed that water-ice grains grow nonspherically when the ambient Ar pressure is below 400 mTorr as seen in Fig. 3. This is also in a good agreement with [13], [14]. The major and minor radii of the water-ice grains grown at 200 mTorr are measured to be 10 and 5 μm , respectively, and thus the aspect ratio is around 2.

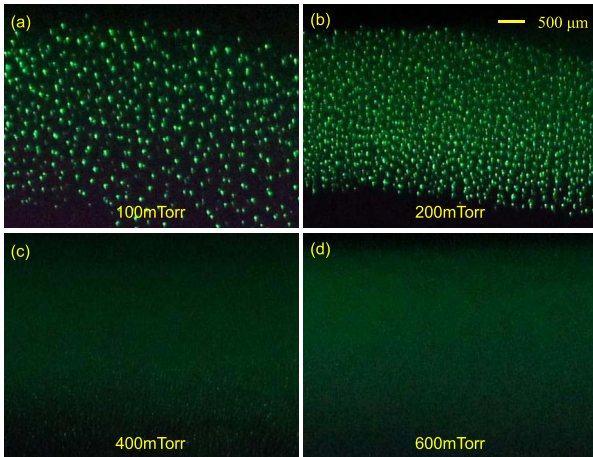


Fig. 3. Photographs of ice grains formed at various Ar ambient gas pressures. The scale bar is shown in the upper right corner.

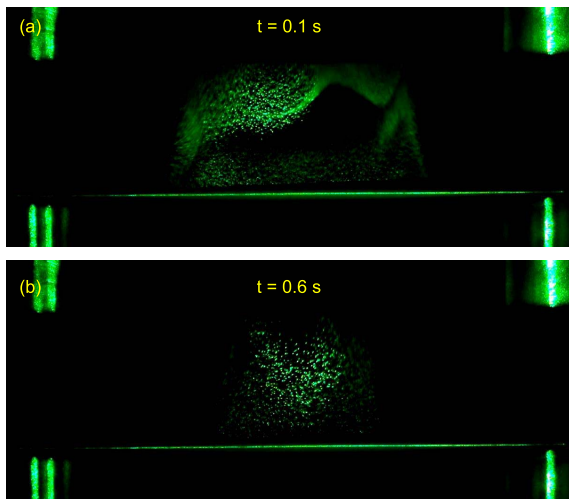


Fig. 4. Still images showing how ice grain clouds evolve after the plasma is off. Ice grains are formed in a plasma ignited by 3-W RF power at 200 mTorr of Ar pressure.

B. Motion of Water–Ice Grains After Plasma Is Turned Off

It is found that the temperature of the top electrode is lower than that of the bottom electrode by 10–20 K if the electrodes are cooled down simultaneously (see Fig. 2). In this case, the ice grains experience the upward Thermophoretic force. In other words, the gravitational force can be partially or completely compensated by the thermophoretic force depending on the temperature difference and the particle radius.

Further experimental studies on the thermophoresis versus gravitational force were conducted as follows: the temperatures of the both electrodes are manipulated by controlling the amount of liquid nitrogen put into the bottom dewar and the top container and captured the motion of ice grains using a digital SLR camera after the plasma was turned off.

Fig. 4(a) and (b) shows still images from a movie. The ice grains shown in Fig. 4 were grown in a plasma ignited by 3 W of RF power at 200 mTorr of Ar pressure and the temperature of the top electrode was lower than that of the bottom electrode by 7.5 K. It is seen that a large fraction of ice grains levitate between the electrodes longer than 0.6 s after the plasma disappears.

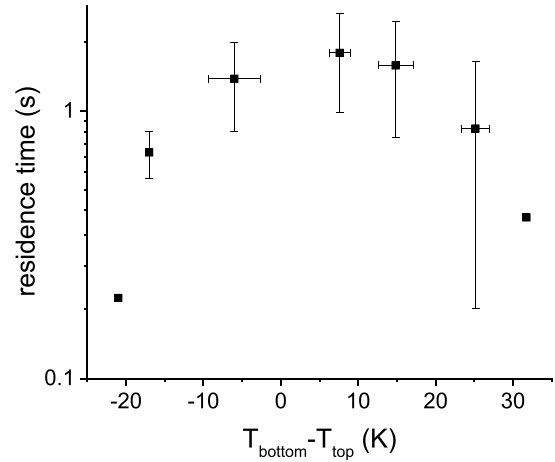


Fig. 5. Ice grain residence time after the plasma is turned off as a function of the temperature difference between the electrodes.

Fig. 5 shows the residence time of water–ice grains after the plasma is turned off as a function of the temperature difference between the electrodes. These temperatures were measured at the electrode rods exposed to the outside of the vacuum chamber by RTDs; the temperatures at the electrode surfaces might be different from the those measured at the electrode rods but the temperature difference between the two electrode rods is believed to be similar to that between the electrode surfaces. The positive values mean the bottom electrode is warmer than that of the top electrode. It was found that when the temperature difference is around 10–15 K, the ice grains levitate the longest, longer than 1 s. On the other hand, when the temperature difference is +30 K or –20 K, ice grains go upward or downward quickly (less than 0.2 s), respectively. Thus, we concluded that the gravitational force is nearly compensated by thermophoresis when the temperature difference is around 10–15 K.

It is useful to calculate the theoretical value of the gravitational and thermophoretic forces. The thermophoretic force suggested by Talbot *et al.* [18] is given by

$$F_{\text{th}} = \frac{32}{15} \frac{r_d^2}{V_{\text{th},n}} \kappa_n \nabla T_n \left(1 + \frac{5\pi}{32} (1 - \alpha) \right) \quad (1)$$

where r_d is the ice grain radius, $V_{\text{th},n}$ is the thermal speed of neutral gas molecules, κ_n is thermal coefficient, T_n is the neutral gas temperature, and α is the accommodation coefficient. Using the measured and nominal values of $r_d = 5 \mu\text{m}$, $T_n = 150 \text{ K}$, $\kappa_n = 0.0124$ for Ar at 200 K, $\alpha \approx 1$, and $\nabla T_n = 15 \text{ K}/1.5 \text{ cm} = 1000 \text{ K/m}$, we obtain $F_{\text{th}} = 3.8 \times 10^{-12} \text{ N}$. The gravitational force is then calculated as

$$F_g = \frac{4\pi r_d^3}{3} \rho g = 4.7 \times 10^{-12} \text{ N}. \quad (2)$$

The calculations show that 80% of the gravitational force is compensated by the thermophoretic force for 5- μm grains when the temperature difference is 15 K which corresponds to our observation. Note that although the ice grains formed in our experiment are not spherical but elongated, the minor radius was used for r_d because: 1) the direction of the ice grain

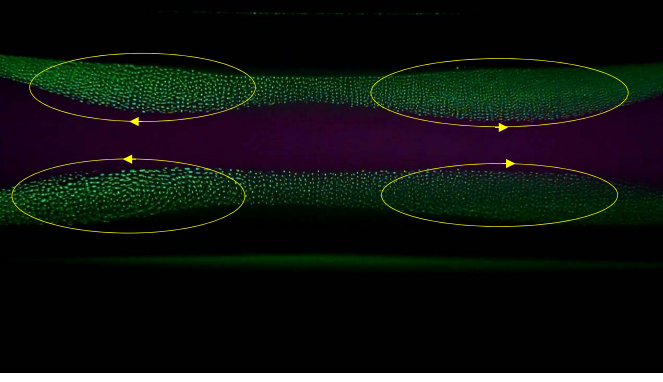


Fig. 6. Still image of a movie captured when there are axisymmetric vortex flows (multimedia file is also available online). The flow speed is measured as $|\mathbf{u}_d| = 6.7 \pm 2.9$ mm/s.

alignment is parallel to that of the temperature gradient so that the cross section for the thermophoretic force is proportional to the minor radius squared and because 2) the mass of ice grains is believed to be lighter than what they seem due to their fractal nature [16] so that using the minor radius gives better mass estimations.

C. Vortex Motion of Ice Grains in a Plasma

Axisymmetric vortex flows are observed after the ice grain growth process ends (but the plasma is still alive) as shown in Fig. 6 (multimedia file is also available online); there are two counter-rotating vortices (the directions of the flows are displayed in Fig. 6 as yellow arrows) in the upper and lower parts of the plasma. The plasma was ignited by 3 W of RF power at 200 mTorr of Ar pressure. The temperature of the top electrode was lower than that of the bottom electrode by 10–15 K so the gravitational force is expected to be nearly compensated by the thermophoretic force (as shown in Section III-B).

The observation of two counter-rotating vortices is somewhat different from the observed quadrupole vortices in the Caltech experiment [19]. One notable difference between the two experiments is that the heat shield was placed around the electrodes in the Caltech experiment but not in the KAERI experiment; the heat shield helps to confine the dust particles in the radial edge region by providing a strong radial electric field near the edge. This explains why we do not see ice grains levitating in the radial edge region compared to the Caltech experiment.

It is clear that the sizes of the ice grains levitating in the upper and lower parts of the plasma are similar. This also supports our previous argument that the gravitational force is nearly compensated by the thermophoretic force.

The origin of vortex flows has been studied by several authors [19]–[21]. In particular, Chai and Bellan analytically (and numerically) showed that vortex flows of ice dust grains in an axisymmetric plasma result from the nonconservative ion drag force. However, they assumed that the electrostatic force is conservative and ignored the neutral gas friction (acting as a damping force for the vortex flows) in the vorticity equation. Thus, herein we propose a more complete picture of the vortex flow analysis.

The poloidal velocity for an incompressible dust fluid \mathbf{u}_d is written as

$$\mathbf{u}_d = \frac{1}{2\pi} \nabla \Psi \times \nabla \phi \quad (3)$$

where $\Psi(r, z)$ is the stream function. Since \mathbf{u}_d flows in the $\{r, z\}$ plane and the system is axisymmetric, $\nabla \times \mathbf{u}_d$ is in the ϕ -direction. By defining a cylindrical vorticity χ as $\chi = r \hat{\phi} \cdot \nabla \times \mathbf{u}_d$ and by operating $r^2 \nabla \phi \cdot \nabla \times$ on (3), we obtain

$$r^2 \nabla \cdot \left(\frac{1}{r^2} \nabla \Psi \right) = -2\pi \chi. \quad (4)$$

The equation of motion of a dust fluid is given by

$$\left(\frac{\partial}{\partial t} + \mathbf{u}_d \cdot \nabla \right) \mathbf{u}_d = \frac{\mathbf{F}}{m_d} - \frac{\nabla P_d}{n_d m_d} + \nu_d \nabla^2 \mathbf{u}_d \quad (5)$$

where \mathbf{F} is the sum of the electrostatic, ion drag, and neutral drag forces, ν_d is the kinematic viscosity of the system. By using the relations $\mathbf{u}_d \times \nabla \times \mathbf{u}_d = (1/2) \nabla (\mathbf{u}_d)^2 - \mathbf{u}_d \cdot \nabla \mathbf{u}_d$ and $\nabla \cdot \mathbf{u}_d = 0$ and by operating $\nabla \phi \cdot \nabla \times$ on (5), we obtain the vorticity equation as

$$\begin{aligned} \frac{\partial}{\partial t} \left(\frac{\chi}{r^2} \right) + \mathbf{u}_d \cdot \nabla \left(\frac{\chi}{r^2} \right) + \gamma_{dn} \left(\frac{\chi}{r^2} \right) \\ = \frac{1}{r} \frac{[\nabla \times (\mathbf{F}_{es} + \mathbf{F}_{id})]_{\phi}}{m_d} + \nu_d \nabla \cdot \left(\frac{1}{r^2} \nabla \chi \right) \end{aligned} \quad (6)$$

where $\gamma_{dn} = 4\pi r_d^2 n_n v_{th,n} m_n / (3m_d)$. Here, we use the Epstein formula for the neutral friction force which is given by [22]

$$\mathbf{F}_n = -m_d \gamma_{dn} \mathbf{u}_d = -(4/3) \pi r_d^2 n_n v_{th,n} m_n \mathbf{u}_d \quad (7)$$

and we do not consider the gravitational and thermophoretic forces because they are conservative by definition as shown in (1) and (2). It is noteworthy that the first term on the right-hand side of (6) is the vorticity source term and the second term is the diffusive dissipation term. In order to see how vortex flows are generated, we need to solve (3), (4), and (6); therefore, we need to calculate $\nabla \times (\mathbf{F}_{es} + \mathbf{F}_{id})$ first.

The electrostatic force \mathbf{F}_{es} can be written as

$$\mathbf{F}_{es} = -e Z_d \mathbf{E} \quad (8)$$

where Z_d is the number of charges residing on a dust grain and \mathbf{E} is the internal electric field in a plasma (i.e., ambipolar electric field). Thus, if Z_d has a dependence on the position $\nabla \times \mathbf{F}_{es}$ may not be conservative. The charge number Z_d can be calculated by the orbital motion-limited (OML) theory which is expressed as

$$\left(\frac{T_i m_e}{T_e m_i} \right)^{1/2} \left[1 - \frac{e V_d}{k_B T_i} \right] \exp \left(\frac{-e V_d}{k_B T_e} \right) = 1 + \frac{Z_d n_d}{n_i} \quad (9)$$

where V_d is the floating potential of the ice grain ($V_d = e Z_d / 4\pi \epsilon_0 r_d$). Note that Z_d is a function of T_e and n_i and thus, Z_d would be a function of positions if n_i depends on the position.

The OML theory is acceptable when the mean free path of the ions is larger than the shielding length and the radius of the dust particle. Our experiment is in this regime because the mean free path of Ar ions (λ_{mf}) at 200 mTorr is 120 μm , and the shielding length of the ice grains (λ_s) is few tens of μm

(depends on the position) while the particle radius is about $5 \mu\text{m}$ so that the third term [23, eq. (31)] is quite smaller than the second term. The ambipolar electric field \mathbf{E} is given by [24]

$$\mathbf{E} = \frac{D_i - D_e}{\mu_i + \mu_e} \frac{\nabla n_i}{n_i} \quad (10)$$

where $D_\sigma = k_B T_\sigma / m_\sigma v_{\sigma n}$ ($\sigma = e, i$) are the electron and ion diffusion coefficients and $\mu_\sigma = |q_\sigma| / m_\sigma v_{\sigma n}$ ($\sigma = e, i$) are the electron and ion mobilities. Here, $v_{\sigma n}$ is the momentum transfer frequency between species σ and n . We assume that dust particles do not change the plasma and the electron temperature of the bulk plasma is isothermal.

The ion drag force suggested by Barns *et al.* [25] is given by

$$\mathbf{F}_{\text{id}} = [b_{\text{coll}}^2 + 2b_{90}^2 \Lambda] \pi n_i m_i v_i \mathbf{u}_i \quad (11)$$

where $b_{\text{coll}} = (1 - ((2eV_d)/(m_i v_i^2)))^{1/2} r_d$, $b_{90} = -(eV_d/(m_i v_i^2)) r_d$, $\Lambda = \ln(((\lambda_s^2 + b_{90}^2)/(b_{\text{coll}}^2 + b_{90}^2)))$, and $v_i^2 = v_{i,\text{tot}}^2 = u_i^2 + v_{\text{th},i}^2$. In our case, since λ_s can be similar to or smaller than b_{coll} in certain regions, the Coulomb logarithm in the orbit cross section might have negative values, which means it is unphysical. Therefore, we adopt the Khrapak's modified Coulomb logarithm expressed as $\Lambda = \ln(((b_{90} + \lambda_s)/(b_{90} + r_d)))$ [26].

The plasma diffusion model gives n_i and u_i as below [24]

$$n_i = n_0 J_0 \left(\frac{\chi_{01} r}{R} \right) \cos \left(\frac{\pi z}{L} \right) \quad \text{with} \quad \frac{v_{iz}}{D_a} = \frac{\chi_{01}^2}{R^2} + \frac{\pi^2}{L^2} \quad (12)$$

$$\mathbf{u}_i = -D_a \frac{\nabla n_i}{n_i} \quad (13)$$

where χ_{01} is the first zero of the Bessel function $J_0(r)$, R is the radius of the electrodes, L is the gap distance between electrodes, D_a is the ambipolar diffusion coefficient, and v_{iz} is the ionization rate. Here, $D_a = (\mu_i D_e + \mu_e D_i) / (\mu_i + \mu_e) \approx T_e D_i / T_i$ is used. Using (12) and (13), we can calculate $\nabla \times \mathbf{F}_{\text{es}}$, $\nabla \times \mathbf{F}_{\text{id}}$, and $\nabla \times (\mathbf{F}_{\text{es}} + \mathbf{F}_{\text{id}})$ and the results of which are shown in Fig. 7(a)–(c), respectively.

The calculations were made in the cylindrical coordinate and so they represent only the right side of the movie. As shown in Fig. 7(a), the electrostatic force is nearly curl-free in the central plasma region but is not conservative near the edge region. However, since our calculation is based on the bulk plasma parameters, a careful interpretation is needed. We think that the plasma-sheath model is required for a precise calculation.

Fig. 7(b) reveals that quadrupole-like curl regions exist in the plasma as previously reported [19], [21]. Note that the radially inner regions have a stronger curl component compared to the radially outer regions. It was also found that both the calculated curls of the orbit force and collection force have a quadrupole feature because both have the same factor, $eV_d/m_i v_i^2$.

Fig. 7(c) shows the calculated $\nabla \times (\mathbf{F}_{\text{es}} + \mathbf{F}_{\text{id}})$; this is put in (6) as Gaussian functions and (3), (4), and (6) are then numerically solved using FlexPDE [27]. The kinematic viscosity ν_d is assumed to be $5 \times 10^{-5} \text{ m}^2/\text{s}$ [28] and $\gamma_{\text{dn}} = 32 \text{ s}^{-1}$. The boundary conditions are no-slip condition

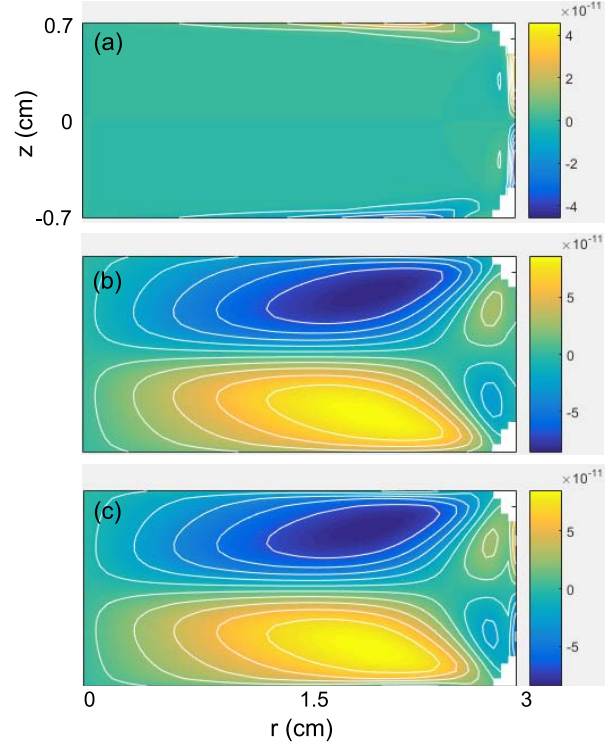


Fig. 7. Calculated (a) $\nabla \times \mathbf{F}_{\text{es}}$, (b) $\nabla \times \mathbf{F}_{\text{id}}$, and (c) $\nabla \times (\mathbf{F}_{\text{es}} + \mathbf{F}_{\text{id}})$. In the calculation, we used $n_0 = 10^{16} \text{ m}^{-3}$, $T_e = 2 \text{ eV}$, $T_i = 150 \text{ K}$, $r_d = 5 \mu\text{m}$, and $n_d = 4 \times 10^{10} \text{ m}^{-3}$.

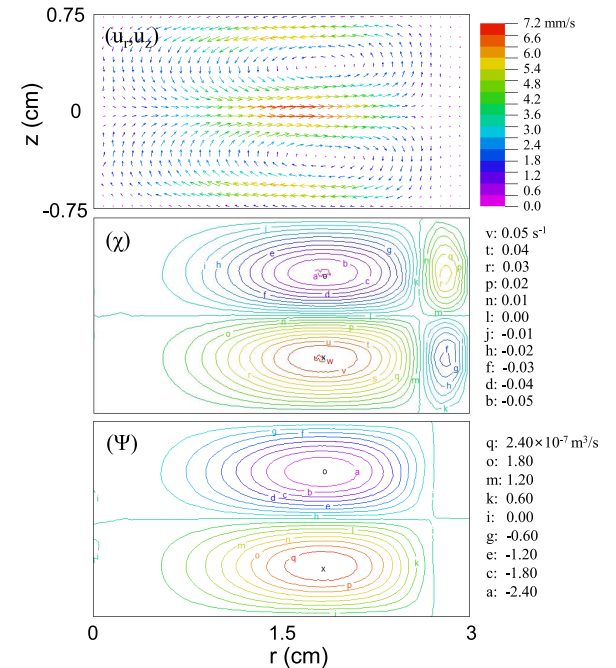


Fig. 8. Calculated (a) poloidal flow velocity (\mathbf{u}_d), (b) cylindrical vorticity (χ), and (c) stream function (Ψ) by FlexPDE [27]. Values of the labeled contours are shown on the right.

and $\chi = \Psi = 0$ at the bottom and top electrodes. The results are displayed in Fig. 8(a)–(c).

Fig. 8(a) shows the calculated poloidal flow velocity; two counter-rotating vortex flows are clearly seen in the radially

inner region whereas two small vortices are barely seen in the radial edge region. Fig. 8(b) and (c) shows χ and Ψ , respectively. The temporal evolution of the FlexPDE calculation reveals that the quadrupole vortex flows are initially formed where the finite $\nabla \times \mathbf{F}$ exists (where the vorticity source exists). This makes the cylindrical vorticity (χ) as (6) describes; χ is diffusively dissipated and damped by the neutral friction. The stream function (Ψ) and the poloidal flows (\mathbf{u}_d) are then induced as depicted in (3) and (4). The inner vortex flows are advected toward the outer region [by the second term on the left-hand side in (6)] and reduce the outer vortex flows. However, since water-ice grains do not levitate in the radial edge region where small vortex flows are predicted to exist, these vortices are not observed from our experiment. The directions of the calculated inner vortex flows are the same as those shown in Fig. 6. The flow speed is also on the order of mm/s corresponding to our observation.

IV. CONCLUSION

A laboratory experiment creating water-ice grains in a plasma environment was successfully built at the KAERI. The apparatus design is similar to the Caltech ice dusty plasma experiment and the several findings from the Caltech experiment are reproduced in the KAERI experiment such as spontaneous nucleation, nonspherical growth, and axisymmetric vortex flows. It is found that the gravitational force exerted on 5 μm ice grains is nearly compensated by the thermophoretic force when the upper electrode is cooler than that of the bottom electrode by 10–15 K. Under this condition, two counter-rotating axisymmetric vortex flows are observed in the upper and lower parts of the plasma. We proposed a more complete picture of vortex flows by including the electrostatic and neutral drag forces in the vorticity equation than that described in [19] and showed that the proposed model successfully predicts vortex flows as we observed from the experiment.

REFERENCES

- [1] M. Hervig, R. E. Thompson, M. McHugh, L. L. Gordley, J. M. Russell, III, and M. E. Summers, "First confirmation that water ice is the primary component of polar mesospheric clouds," *Geophys. Res. Lett.*, vol. 28, no. 6, pp. 971–974, 2001.
- [2] C. K. Goertz, "Dusty plasmas in the solar system," *Rev. Geophys.*, vol. 27, no. 2, pp. 271–292, 1989.
- [3] D. A. Mendis and M. Horányi, "Dusty plasma effects in comets: Expectations for Rosetta," *Rev. Geophys.*, vol. 51, no. 1, pp. 53–75, 2013.
- [4] M. Rapp and F.-J. Lübken, "Polar mesosphere summer echoes (PMSE): Review of observations and current understanding," *Atmos. Chem. Phys.*, vol. 4, pp. 2601–2633, Dec. 2004.
- [5] M. Rapp, G. E. Thomas, and G. Baumgarten, "Spectral properties of mesospheric ice clouds: Evidence for nonspherical particles," *J. Geophys. Res., Atmos.*, vol. 112, Feb. 2007, Art. no. D03211.
- [6] O. Havnes *et al.*, "First detection of charged dust particles in the Earth's mesosphere," *J. Geophys. Res., Space Phys.*, vol. 101, pp. 10839–10847, May 1996.
- [7] L. A. Frank, B. G. Burek, K. L. Ackerson, J. H. Wolfe, and J. D. Mihalov, "Plasmas in Saturn's magnetosphere," *J. Geophys. Res., Space Phys.*, vol. 85, pp. 5695–5708, Nov. 1980.

- [8] W.-H. Ip, "Thermal plasma composition in Saturn's magnetosphere," *Planet. Space Sci.*, vol. 48, pp. 775–783, Jun. 2000.
- [9] C. C. Porco *et al.*, "Cassini observes the active south pole of Enceladus," *Sci.*, vol. 311, pp. 1393–1401, Mar. 2006.
- [10] J. K. Davies *et al.*, "The detection of water ice in comet Hale-Bopp," *Icarus*, vol. 127, no. 1, pp. 238–245, 1997.
- [11] J. L. Burch, T. I. Gombosi, G. Clark, P. Mokashi, and R. Goldstein, "Observation of charged nanograins at comet 67P/Churyumov-Gerasimenko," *Geophys. Res. Lett.*, vol. 42, pp. 6575–6581, Aug. 2015.
- [12] M. Horanyi and D. A. Mendis, "Trajectories of charged dust grains in the cometary environment," *Astrophys. J.*, vol. 294, pp. 357–368, Jul. 1985.
- [13] K.-B. Chai and P. M. Bellan, "Spontaneous formation of nonspherical water ice grains in a plasma environment," *Geophys. Res. Lett.*, vol. 40, pp. 6258–6263, Dec. 2013.
- [14] K.-B. Chai and P. M. Bellan, "Study on morphology and growth of water-ice grains spontaneously generated in a laboratory plasma," *J. Atmos. Solar-Terrestrial Phys.*, vol. 127, pp. 83–91, May 2015.
- [15] K.-B. Chai and P. M. Bellan, "Formation and alignment of elongated, fractal-like water-ice grains in extremely cold, weakly ionized plasma," *Astrophys. J.*, vol. 802, no. 2, 2015, Art. no. 112.
- [16] R. S. Marshal, K.-B. Chai, and P. M. Bellan, "Identification of accretion as grain growth mechanism in astrophysically relevant water-ice dusty plasma experiment," *Astrophys. J.*, vol. 837, no. 1, 2017, Art. no. 56.
- [17] L. S. Matthews, V. Land, and T. W. Hyde, "Charging and coagulation of dust in protoplanetary plasma environments," *Astrophys. J.*, vol. 744, no. 1, 2012, Art. no. 8.
- [18] L. Talbot, R. K. Cheng, R. W. Schefer, and D. R. Willis, "Thermophoresis of particles in a heated boundary layer," *J. Fluid Mech.*, vol. 101, pp. 737–758, Dec. 1980.
- [19] K.-B. Chai and P. M. Bellan, "Vortex motion of dust particles due to non-conservative ion drag force in a plasma," *Phys. Plasmas*, vol. 23, no. 2, 2016, Art. no. 023701.
- [20] M. Schwabe and D. B. Graves, "Simulating the dynamics of complex plasmas," *Phys. Rev. E, Stat. Phys. Plasmas Fluids Relat. Interdiscip. Top.*, vol. 88, no. 2, 2013, Art. no. 023101.
- [21] T. Bockoldt, O. Arp, K. O. Menzel, and A. Piel, "On the origin of dust vortices in complex plasmas under microgravity conditions," *Phys. Plasmas*, vol. 21, no. 10, Art. no. 103703, 2014.
- [22] P. S. Epstein, "On the resistance experienced by spheres in their motion through gases," *Phys. Rev.*, vol. 23, p. 710, Jun. 1924.
- [23] M. Lampe *et al.*, "Trapped ion effect on shielding, current flow, and charging of a small object in a plasma," *Phys. Plasmas*, vol. 10, no. 5, pp. 1500–1513, 2003.
- [24] M. A. Lieberman and A. J. Lichtenber, *Principles of Plasma Discharges and Materials Processing*, 2nd ed. Hoboken, NJ, USA: Wiley, 2005.
- [25] M. S. Barnes, J. H. Keller, J. C. Forster, J. A. O'Neill, and D. K. Coultas, "Transport of dust particles in glow-discharge plasmas," *Phys. Rev. Lett.*, vol. 68, no. 3, pp. 313–316, 1992.
- [26] S. A. Khrapak, A. V. Ivlev, G. E. Morfill, and H. M. Thomas, "Ion drag force in complex plasmas," *Phys. Rev. E, Stat. Phys. Plasmas Fluids Relat. Interdiscip. Top.*, vol. 66, no. 4, p. 046414, 2002.
- [27] PDE Solutions Inc., *FlexPDE™*. Accessed: May 1, 2017. [Online]. Available: <http://www.pdesolutions.com/index.html>
- [28] G. E. Morfill *et al.*, "Highly resolved fluid flows: 'Liquid plasmas' at the kinetic level," *Phys. Rev. Lett.*, vol. 92, no. 17, 2004, Art. no. 175004.



Kil-Byoung Chai received the B.A. and Ph.D. degrees in plasma physics from the Korea Advanced Institute of Science and Technology, Daejeon, South Korea, in 2005 and 2011, respectively.

He was a Post-Doctoral Fellow with the Bellan Plasma Group, California Institute of Technology, Pasadena, CA, USA. In 2016, he joined Korea Atomic Energy Research Institute, Daejeon, South Korea. His current research interests include dusty plasma physics, MHD-driven flows, and optical emission spectroscopy.